Force Spectroscopy of the Double-Tethered Concanavalin-A Mannose Bond

Timothy V. Ratto,* Kevin C. Langry,* Robert E. Rudd,† Rodney L. Balhorn,‡ Michael J. Allen,§ and Michael W. McElfresh*

*Chemistry and Materials Science, †Physics and Advanced Technologies, and ‡Biology and Biotechnology Research Program, Lawrence Livermore National Laboratory, Livermore, California 94550; and §Biometrology Inc., Alameda, California 94501

ABSTRACT We present the measurement of the force required to rupture a single protein-sugar bond using a methodology that provides selective discrimination between specific and nonspecific binding events and helps verify the presence of a single functional molecule on the atomic force microscopy tip. In particular, the interaction force between a polymer-tethered concanavalin-A protein (ConA) and a similarly tethered mannose carbohydrate was measured as 47 ± 9 pN at a bond loading rate of ~10 nN/s. Computer simulations of the polymer molecular configurations were used to determine the angles that the polymers could sweep out during binding and, in conjunction with mass spectrometry, used to separate the angular effects from the effects due to a distribution of tether lengths. We find that when using commercially available polymer tethers that vary in length from 19 to 29 nm, the angular effects are relatively small and the rupture distributions are dominated by the 10-nm width of the tether length distribution. In all, we show that tethering both a protein and its ligand allows for the determination of the single-molecule bond rupture force with high sensitivity and includes some validation for the presence of a single-tethered functional molecule on the atomic force microscopy tip.

INTRODUCTION

Molecular recognition in biological systems, such as between receptors and ligands or proteins and antibodies, is the first step in a wide variety of biological functions (McDonnell, 2001). This often rate-limiting process is commonly investigated utilizing molecules free in solution (Lavigne and Anslyn, 2001) or directly affixed to a solid support (McDonnell, 2001); however, a great number of biological molecules are in fact attached to the ends of flexible or semiflexible tethers (Wong et al., 1997; Davis et al., 2003; Zhao et al., 2001) and it is natural to ask how the tethers affect binding properties and whether artificial tethers can be used to an advantage in measuring intrinsic receptor-ligand interactions. The tethers serve both to extend the molecule away from the cellular membrane, and to limit the volume within which interactions can occur, and may have additional unknown functions. It has been shown that measuring equilibrium molecular binding properties such as affinities, where at least one of the species is free in solution, does not scale well with the binding properties of cell surface tethered molecules, where movement is largely restricted to the two-dimensional plane of the membrane (Zhu, 2000; Riper et al., 1998; Chang and Hammer, 1999). Additionally, a recent study revealed that the kinetics of interactions between a polymer-tethered protein and its ligand were heavily influenced by relatively rare extensions of the polymer tether, indicating that molecular tethers can have effects that are not well explained by analyzing equilibrium measurements (Jeppesen et al., 2001).

Force spectroscopy has recently emerged as a powerful technique for measuring binding properties of biological interactions at the single molecule level (Zlatanova et al., 2000; Chen and Moy, 2002). This nonimaging mode utilizes biological molecules attached to an atomic force microscopy (AFM) cantilever, which is then used to probe an either naturally, as with cell membranes, or artificially, ligand-functionalized surface. The AFM cantilever is moved close enough to the surface for the molecules to bind and then retracted at a constant velocity. By monitoring the deflection of the cantilever during the approach-retraction cycle the extension length and bond rupture force can be ascertained (Liu et al., 1999; Benoit et al., 2000; Clausen-Schaumann et al., 2000; Conti et al., 2002; Florin et al., 1994; Hugel and Seitz, 2001; Ludwig et al., 1994; Merkel, 2001). Attaching the binding species with polymer tethers and correlating bond rupture with the distance the polymer is stretched before rupture also allows the differentiation of specific from nonspecific bond formation (Riener et al., 2003) and, in conjunction with computer simulations, can provide information about the molecular configurations (e.g., protein number and tether length) of both the probe and the sample surface. Previous investigations utilizing tethered molecules have focused mainly on a more qualitative discussion of the effects on the force curve due to the tether, such as allowing oriented coupling due to the increased mobility of the protein, and separating specific interactions from nonspecific tip-substrate adhesion.

Here we present a systematic analysis of the specific effects on the binding between two tethered molecules due to the presence of the tethers. A single-tethered system, i.e., tethering a molecule on the AFM tip, helps decrease nonspecific

Submitted September 9, 2003, and accepted for publication December 29, 2003.

Address reprint requests to Timothy V. Ratto, Tel.: 925-422-8739; Fax: 925-422-1487; E-mail: ratto7@llnl.gov.

0006-3495/04/04/2430/08 $2.00

binding by moving the specific interaction away from the surface of the AFM tip. However, as we show, nonspecific interactions between the molecules on the tethers and substrate or tip-bound molecules are still quite probable and significantly decrease the reliability of the measurement. In this study we attach both the protein to the AFM tip as well as the ligand to the substrate using polymer tethers. Tethering both molecules has the added advantage of moving the specific interactions away from both the tip surface and the substrate surfaces. This improves the fidelity of the force measurements because any molecules that may contribute to nonspecific binding, either those making up the tip or substrate or bound to it, are not nearby. Additionally, and more importantly, double tethering allows us to localize both specific and nonspecific binding to particular distance ranges along a force curve and measure the distribution of bond rupture forces involved. This, in addition to modeling coupled with mass spectrometry, allows us to confirm the presence of a single tether, and thus a single functional molecule, on the AFM tip. To our knowledge, this is the first force spectroscopy study that utilizes a well-characterized double-tethered system and directly correlates the specific and nonspecific bond rupture forces with the rupture distance. Besides increasing the reliability of the specific bond rupture force measurement, using a double tether allows the nonspecific bond rupture forces to be measured. This information can, in turn, be of great value in reducing nonspecific binding and therefore optimizing the experimental system.

In this study, we investigate the bond rupture force between concanavalin A (ConA) and mannose. ConA is a lectin, or carbohydrate-binding protein, and has been well characterized using crystallography and other methods (Mann et al., 1998; McDonnell, 2001; Kanellopoulos et al., 1996). Carbohydrate binding serves as the initial step in a wide variety of biological functions, ranging from fertilization to viral infection (Varki, 1993) and expanding the understanding of the mechanisms behind carbohydrate recognition will assist in the development of new strategies for understanding biological function and combating disease. Although previous force spectroscopy studies measuring the interaction between ConA and mannose have been described (Gad et al., 1997; Touhami et al., 2003), the distribution of forces attributed to the single-molecule ConA-mannose bond rupture was larger than we report here. We ascribe the smaller force range we measure to be due to the exclusion of most nonspecific interactions, as well as possibly the result of measuring single ConA-mannose bond ruptures rather than multiple interactions simultaneously.

MATERIALS AND METHODS

General

Chemicals were obtained from Sigma-Aldrich Chemicals (St. Louis, MO) unless noted otherwise. Chloroform (99.8%, stabilized with amylenes) was used as obtained. Anhydrous dimethylformamide was degassed at room temperature by stirring for 30 min under a vacuum of 10 mm Hg before use. Methyltriethoxysilane and 3-aminopropyl-triethoxysilane were distilled before use.

Tip functionalization

New silicon nitride cantilevers stored under nitrogen were used without additional cleaning. Cantilevers were silanized from the vapor phase using recently distilled 3-aminopropyl-triethoxysilane (APTES) and methyltriethoxysilane (MTES) at an amino/methyl ratio of 1/250 to reduce the number of active groups on the tip. The silanization was allowed to progress overnight, after which time the tips were removed and heated for 10 min at 110°C in air. The tips were cooled, immersed for 30 min in chloroform containing 10 mg/mL of α,ω-diNHS-poly(ethylene glycol) with a nominal molecular weight of 3400 amu $(PEG\text{-}(SPA)_2)$, 4M4M0F02, Shearwater Polymers, Huntsville, AL; now Nektar Therapeutics, www.nektar.com), corresponding to a nominal extended length of ~25 nm. The tips were rinsed with chloroform, dried with nitrogen, and immediately immersed in 25 mM phosphate buffer solution, pH 8.0, containing 2 mg/mL ConA (*Canavalia ensiformis*, Jack Bean, Type VI, Sigma). After 20 min, the tips were removed and rinsed briefly with 25 mM phosphate buffer, pH 8, and then for 10 min with three volumes of 25 mM phosphate buffer, pH 5.0. Because ConA is a dimer below pH 7 this step is necessary to remove the tetrameric form of ConA, as well as any larger aggregates. The derivatized tips were used within several hours of their preparation.

Substrate functionalization

Ethanol-rinsed gold-coated (gold thickness 1000 Å) silicon (Platypus Technologies, LLC, Madison, WI) was immersed in ethanol containing 1 mM 16-mercaptohexadecanoic acid for 30 min. The resulting self-assembled monolayers (SAMs) were rinsed first with ethanol and then with four volumes of chloroform. The SAMs were then immersed in chloroform containing 10 mg/mL 1,1′-carbonyldiimidazole for 30 min and then immediately rinsed in four volumes of chloroform before being immersed in chloroform containing 10 mg/mL of α,ω-diamino-polyethylene glycol with a nominal molecular weight of 3400 amu $(PEG\text{-}(amine)_2)$, 2V2V0F22, Shearwater Polymers, Huntsville, AL). The SAMs were rinsed in four volumes of chloroform, dried with nitrogen, and immersed for 1 h in dimethylformamide containing 6 mg/mL α-D-mannopyranosylphenyl isothiocyanate (Sigma) under an atmosphere of dry nitrogen. The SAMs were rinsed sequentially with ethanol and water, and then dried with nitrogen. The derivatized SAMs were used within hours of their preparation.

All points of attachment between the protein and the tip and the ligand and the substrate consist of covalent bonds. At bond-loading rates comparable to the rates we use in this study, covalent attachments have bond-rupture forces in excess of 1000 pN (Grandbois et al., 1999), thus we can be confident that the rupture forces we measure are not due to the polymer tethers being removed from either the tip or the substrate.

Mass spectrometry

Matrix-assisted laser desorption ionization (MALDI) time of flight (MALDI-TOF) mass spectrometry was performed using a PerSeptive Biosytems Voyager-DE STR biospectrometry workstation (Foster City, CA) equipped with a nitrogen laser (337-nm emission). The instrument was calibrated with angiotensin and the B-chain of bovine insulin with the flight pattern for positive ions configured in the reflectron mode. Other relative parameters include: the source voltage, 20 kV; grid voltage, 64.8%; the extraction delay time, 315 ns; and the sample matrix, α-cyano-4-hydroxycinnamic acid.

Force spectroscopy

A Nanoscope IIIa (Digital Instruments, Veeco, Santa Barbara, CA) was used to control a commercial Bioscope AFM (Digital Instruments, Veeco) in force calibration mode. Deflection versus vertical-distance measurements were performed at a 1-Hz scanning frequency and at amplitudes of 100 nm. To minimize deviations between experiments, a relative trigger of 5–10 nm was used on all deflection-distance curves that served to limit both the force that the tip applied to the surface and the tip-surface contact area. In addition, upon activation of the trigger, the tip was held at the sample surface for 1 s to allow the tethered proteins to form bonds with tethered ligands. The 1-s delay also allowed us to make certain that any differences seen in bond-rupture force were not a consequence of the protein and/or ligand having variable times for achieving optimum spatial orientations. All measurements were carried out in pH 6.0 buffer containing 50 mM *N*, *N*-dimethylglycine, 100 mM NaCl, 1.0 mM $CaCl_2$, and 1.0 mM $MnCl_2$. The spring constants of the standard Si_3N_4 cantilevers (Veeco) were calibrated using the thermal noise method in fluid (Florin et al., 1995; Hutter and Bechhoefer, 1993; Butt and Jaschke, 1995). A spectrum analyzer (760a, Scientific Instruments, Palo Alto, CA) was used to measure the unfiltered signal of the thermally excited cantilever noise. Spring constants ranging from 0.075 to 0.14 N/m for the 100-μm levers were obtained from the integral of the first resonance peak in the power spectral density plot. We estimate the absolute uncertainty of the spring constant calibration to be ~20%.

Data analysis

Cantilever deflection versus distance curves were analyzed using Igor Pro (WaveMetrics, Lake Oswego, Oregon) and a collection of macros written for Igor Pro by Dmitri Venezov, modified here to facilitate bond-rupture detection. The modified macros essentially take the first derivative of the deflection versus distance curves and search the resulting data for abrupt changes in slope. False positives are decreased by filtering the initial data with a low-pass filter and requiring that the change in slope for a positive result be larger than four times the change in slope due to random vibrations of the cantilever. The cantilever deflection measurements are converted to force values using the slope of the cantilever on a hard surface and the cantilever spring constant determined as above. Bond-rupture distances are determined from the deflection versus distance curves as the point at which the tip contacts the hard substrate, subtracted from the point at which a negative deflection returns to zero. This is essentially the distance between the AFM tip and the substrate when both the tethered protein and tethered ligand are fully extended.

RESULTS

Rupture distances

AFM direct-force measurements were acquired to characterize both the strength of the adhesive interactions between the polymer-tethered ConA protein and the mannose functionalized substrate, and the bond-rupture distance at which the interactions took place. We found adhesive interactions clustering at three characteristic length scales, <10 nm, between 10 and 33 nm, and between 33 and 43 nm, as shown in Fig. 1, in comparison with the nominal PEG length of 25 nm. Fig. 1 *A* shows a representative interaction occurring close to the point of contact between the AFM tip and the substrate, Fig. 1 *B* shows an additional interaction at a tip-substrate distance of ~20 nm, and Fig. 1 *C* shows an additional interaction at a tip-substrate distance of ~40 nm. This latter interaction at about twice the PEG length is the proposed specific interaction between the tethered ConA and the tethered mannose, as depicted in the schematic diagram in Fig. 1.

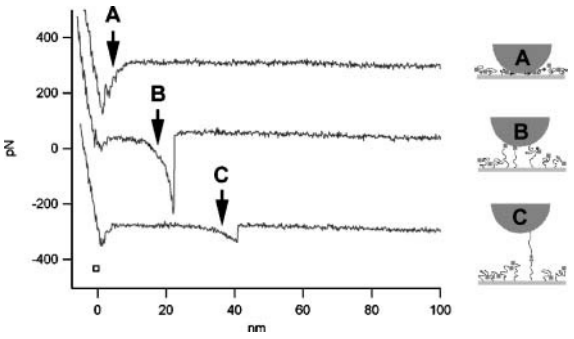

FIGURE 1 Experimental AFM retraction curves and schematics showing interactions at three characteristic distances. (*A*) Proposed nonspecific tip-substrate interactions (<10 nm); (*B*) proposed nonspecific tip-ligand interactions (between 10 and 33 nm); and (*C*) proposed specific protein-ligand interactions (between 33 and 43 nm). Note that the zero point along the *x* axis denotes the point of contact between the tip and the substrate. Force curves *A* and *C* have been rescaled in the *y* axis to fit all three curves on one graph.

Mass spectrometry

To assess the contribution to the rupture distance due to the lack of monodispersity in the polymer tether lengths, the distribution of tether lengths was measured using MALDI-TOF mass spectrometry. The data are presented as a table (published as Table 1 in the supporting information; see Supplementary Material) together with the calculated mass for a PEG with a molecular composition of $H_2N(CH_2CH_2O)_nCH_2CH_2NH_2$ where *n* is the number of monomer units. From the mass data, a range of polymer lengths were derived and ranged from ~20-nm to 30-nm long as shown in Fig. 2. This length is based on a monomer unit length of 3.36 Å and assumes a fully extended PEG in its lowest energy conformation. Specific interactions occur over a distance

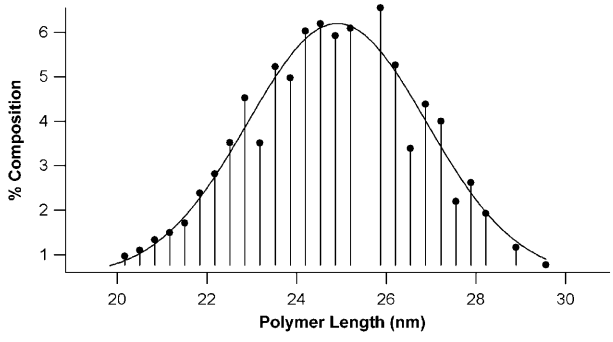

FIGURE 2 Length distribution of the α,ω-diamino PEG polymer tethers with a nominal mass of 3400 amu measured by MALDI. The solid line is a best-fit Gaussian with a distribution of 25 nm ± 2.8 nm.

range of 33–43 nm, a value that is consistent with the ~10-nm width of the length distribution of the polymer tethers.

Specific bond-rupture forces

To establish criteria for the determination of specific versus nonspecific interactions we obtained sets of deflection versus distance curves using a variety of functionalized tips and found that if data taken with more than one tip were mixed before analysis, it became difficult to determine bond-rupture distances, most likely due to variability in tip functionalization. For this reason we analyzed over 500 adhesive interactions from a set of deflection versus distance curves taken using a single functionalized AFM tip. Histograms of the frequencies of adhesive interactions at tip-substrate distances between 1 and 50 nm for a ConA functionalized tip on a mannose functionalized substrate are shown in Fig. 3 *A*. The same data are graphed as the rupture force versus tip-substrate distance in Fig. 3 *C* to show how the rupture forces are clustered as a function of tip-substrate distance. We find that the most frequent rupture force for the single-molecule ConA-mannose bond is 47 ± 9 pN at a bond-loading rate of ~10 nN/s. To demonstrate that the observed adhesive interactions seen between 33 and 43 nm are indeed due to specific ConA-mannose bond rupture, we replaced the working buffer with buffer containing 5 mM α-D-mannose, known to be a competitive inhibitor of ConA. Competitive inhibition of binding is commonly used as an indicator of protein-ligand specificity. The adhesive interactions between 33 and 43 nm were almost completely eliminated by the presence of the blocking agent whereas the interactions below 33 nm were mostly unaffected (see Fig. 3, *B* and *D*).

DISCUSSION

Several features of the large cluster of interactions between 33 and 43 nm seen in Fig. 3 *A* indicate these rupture forces correspond to the breaking of specific protein-carbohydrate bonds that form between a single-tethered protein on the tip and the tethered ligands on the substrate. First, the interactions are clustered around 40 nm, greater than the length of a single tether but less than the additive length of two tethers. Second, this cluster was not seen in either the experiment in which the ConA-mannose interaction was blocked by the addition of free mannose into the buffer solution (Fig. 3 *C*) or when an unfunctionalized tip was used to probe the substrate. The width of the cluster of interactions can be directly attributed to the 10-nm wide distribution of polymer lengths as measured by MALDI, which is representative of the length distribution of the polymer-tethered ligands on the substrate. If there were more than one tethered protein on the AFM tip we should have observed either additional clusters of interactions at different locations along the force curve or a much broader cluster reflecting the differing locations of the tethers along the radius of curvature of the AFM tip. Finally, the rupture forces for the interactions between 33 and 43 nm are clustered around 47 ± 9 pN (Fig. 4 *A*), whereas the rupture forces for the interactions between 5 and 33 nm show a much broader distribution of values, ranging from ~20 to 350 pN (see Fig. 4, *B* and *C*). Thus, we can state with some certainty that the fraction of measurements represented by the 33–43-nm cluster consists of specific bonding events between a single ConA and mannose, however, there may be other specific bonding events that lie outside the cluster.

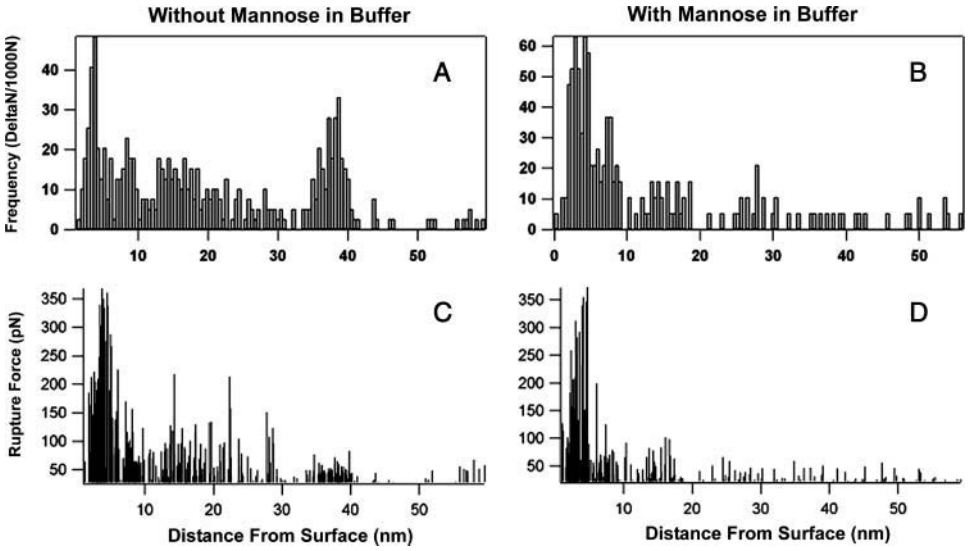

FIGURE 3 Histograms of the frequency of interactions (*A* and *B*) and magnitude of the rupture forces (*C* and *D*) at increasing distances from the point of contact between the AFM tip and the surface. *A* and *C* show the specific interactions between the ConA and mannose at the characteristic lengths between 33 and 43 nm. When the buffer solution in the AFM liquid cell is exchanged with buffer-containing free mannose, binding between the ConA on the AFM tip and the mannose attached to the substrate is blocked, and the specific interactions seen at the characteristic lengths between 33 and 43 nm can no longer be seen (*B* and *D*). Note that the number of interactions at lengths <33 nm also decreases upon addition of free mannose, implying that specific interactions may also occur at these lengths. These may be due to the tethered protein adhering to the AFM tip or tethered ligands adhering to the substrate before the formation of a bond.

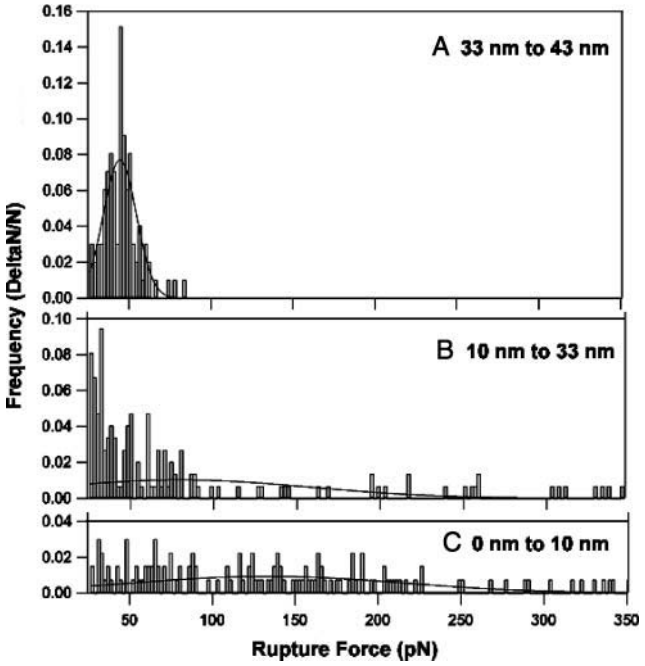

FIGURE 4 Frequency versus force histograms showing the distribution of forces from the three characteristic regions of the force curves. (*A*) Shows the distribution of forces measured between 33 and 43 nm from the point of contact between the tip and substrate. A Gaussian best fit to the histogram reveals the proposed single molecule most frequent rupture force for the ConA-mannose interaction of 47 ± 9 pN. The distributions of forces for the other two length scales are much broader, varying between ~20 and 350 pN. Note that these forces were measured at bond loading rates of 10nN/s.

Single-molecule force spectroscopy measurements of the ConA-mannose bond rupture force have been attempted previously. One paper reported that the single-bond rupture force was 96 ± 55 pN (Touhami et al., 2003) at a loading rate of 4 nN/s whereas an earlier article reported the value to be between 75 and 200 pN (Gad et al., 1997). The decrease to <1/5 the width of the previously reported force ranges (>100 pN compared to 19 pN) is almost certainly due to our exclusion of the majority of nonspecific interactions. Also, in both cases it is likely that the authors were measuring multivalent ConA-mannose bond ruptures rather than the single-molecule measurement because the previous experiments were carried out above pH 7.2. Above pH 7, ConA is found in its tetrameric form (Kanellopoulos et al., 1996). The differing loading rates may also play a role, as bond rupture forces have been shown to be loading-rate dependent (Evans, 2001; Friedsam et al., 2003; Kienberger et al., 2003; Riper et al., 1998).

Distribution breadths

There are several effects that contribute to the breadth of the force and rupture location distributions observed. One contribution is a result of the distribution of PEG tether lengths. A second contribution comes from the geometry of the binding pair, because the point at which the PEG attaches to the AFM tip may be offset laterally from the point of attachment of the second PEG to the substrate. Fig. 5 shows a schematic of the molecular configuration of the interaction. As the AFM tip is retracted, the PEGs straighten leading to a configuration at the point of rupture that is tilted from the vertical by an angle θ. The angle changes the apparent rupture force, F_{apparent}, and length, l_{apparent}, according to $F_{\text{apparent}} = F_{\text{intrinsic}}\cos(\theta)$ and $l_{\text{apparent}} = l_{\text{intrinsic}}\cos(\theta)$. Also note that the apparent strain rate is affected: $\dot{l}_{\text{apparent}} = \dot{l}_{\text{intrinsic}}\cos(\theta)$, where the dot signifies the rate of change in time. Suppose we make a standard ansatz that the intrinsic rupture force is proportional to a power of the strain rate for, $F_{\text{intrinsic}}(\dot{l}) \propto \dot{l}^{\beta}$; then the apparent force is further affected according to $F_{\text{apparent}} = F_{\text{intrinsic}}(\dot{l}_{\text{apparent}})\cos(\theta)^{1-\beta}$. This is particularly interesting because Evans and others have argued that typically $\beta = 1$, the angle-independent case (Evans, 2001). Thus, any angle dependence of the force is a measure of the departure from canonical scaling. However, it should be noted that $\beta = 1$ is only a general trend, and the force spectrum typically shows significant structure about the general trend of $\beta = 1$.

The formulas we have just presented assume that the angle at rupture is known, but in practice there is no simple way to measure the angle during a force-distance measurement. Instead we employ modeling to understand the statistical probability distribution of angles at rupture and its impact on the measured length and force distributions. This probability distribution is reflected in the distribution of rupture forces and length due to the geometry of the binding pair. Fig. 6 contains the angle distributions for two PEGs of the same

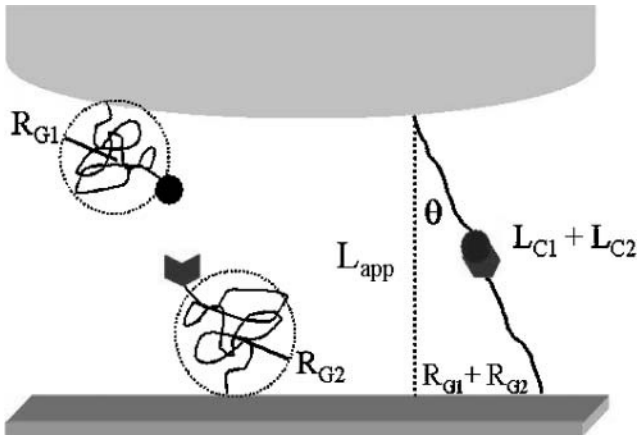

FIGURE 5 A schematic of the molecular configuration of the binding system. R_{G1} and R_{G2} are the radius of gyration of the polymers on the tip and substrate. θ is the angle that the extended polymers make to the vertical. L_{C1} and L_{C2} are the fully extended contour lengths of the polymers on the AFM tip and the polymers on the substrate, respectively. L_{app} is the projection of the extended linked polymers along the vertical axis. Note that because we only measure the change in position along the vertical axis when acquiring data in force mode, L_{app} is the apparent length at which we measure interactions. L_{app} is dependent on the angle, θ, as well as L_{C1} and L_{C2}.

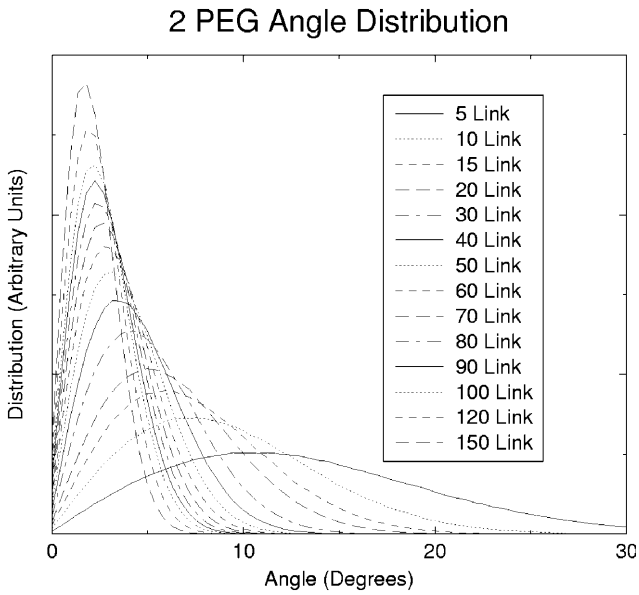

FIGURE 6 The distribution of bond angles at the instant of bond rupture calculated using a freely jointed polymer model for each PEG, assuming monodisperse PEG lengths and full extension. The peak in the distribution is determined by the ratio of the radius of gyration of the polymer on the surface to the polymer length (in particular, it is the arc-cosine of this ratio). As the contour length of the PEG (measured in units of the persistence length, i.e., links in the model) increases, the ratio decreases as $1/\sqrt{N}$, where N is the number of links. This trend to small angles suggests that long PEG tethers act to limit unwanted angle dispersion effects.

length from a Monte Carlo simulation, measured in terms of the persistence length or ''links.'' The PEG persistence length is the size of one monomer. The modeling is based on a freely jointed chain model, constrained to remain on one side of the substrate and outside the AFM tip, but otherwise free to self-intersect. End hiding phenomena were neglected, as were polymer thickness effects such as knotting. A worm-like chain model would show similar trends. Each curve represents the probability distribution arising from 100,000 Monte Carlo samples.

The trend in the angle distributions is for narrower peaks at smaller angles as the PEG length increases. This trend is consistent with the expectation that the binding end of the PEG will spend most of its time within its radius of gyration, R_G, a quantity that grows like $\sqrt{N}$ where N is the number of links in the chain. The root-mean-square of the sine of the binding angle is then proportional to $\sqrt{N}/N$ or $1/\sqrt{N}$. Thus in the limit of long chains (large N), the angles become small. This trend is depicted quantitatively through the peaks in the distributions coming from the freely jointed chain model plotted in Fig. 6.

With some additional development it might be possible to calculate the probability distributions analytically. To facilitate further analysis and to provide the data in a compact form, we have fit the distributions to an analytic form. The angle distributions are fit well by a modified Gaussian form $f(\theta) = [(A + BN)\theta + D(N)\theta^2]e^{-CN\theta^2}$, where A, B, and C are constants, and $D = 2[2CN - (A + BN)]\sqrt{CN/\pi}$, determined by normalization. The values for these coefficients determined by a least-squares fit are $A = -0.0043$, $B = 0.0023$, and $C = 0.00076$ with the angles measured in degrees. Given the angular distribution, the apparent length distribution is given by, $\tilde{f}(l_{\text{apparent}}) = \sum_i P_i f(\theta(l_{\text{apparent}}))/\sqrt{l_i^2 - l_{\text{apparent}}^2}$, where P_i is the probability of bonding to the i^{th} kind of substrate PEG such that the total length of the PEG pair is l_i. By convention $f(\theta(l_{\text{apparent}}))$ is taken to be zero if $l_{\text{apparent}} > l_i$. This apparent length distribution is plotted in Fig. 7. The result is a length distribution whose width is dominated by the intrinsic width in the PEG length distribution, spread by only $\sim$1 nm due to the angle distribution for the long polymer chains of interest consisting of $\sim$77 monomers each. The width of the measured length distribution in the 33–43-nm peak is in good agreement with the Monte Carlo model using PEG length estimates obtained from the MALDI mass spectrometry measurements, further supporting the conclusion that the peak is due to specific binding events.

It is possible that the cluster of interactions between 33 and 43 nm in Fig. 3 *A* is due to multiple polymer tethers on the AFM tip, rather than only one as we have depicted in the schematic representation shown in Fig. 1. Multiple tethers would result in a broader distribution of lengths, due to the lack of length monodispersity in the synthesized polymers (as shown in the MALDI data), and also from the variable location of the tethers along the radius of the tip itself. Multiple tethers contributing to the distributions measured in this study are unlikely, however, as even one other polymer tether on the tip would broaden the distribution significantly, unless it was the same length and attached at the same distance up the side of the tip as the other polymer. Another possibility is that the distribution is indeed due to one single tether but that transient higher-order structures exist within the polymer itself. Knot theory applied to the topology of macromolecules indicates that the simple trefoil or ''overhand'' knot can be present in any long polymer strand

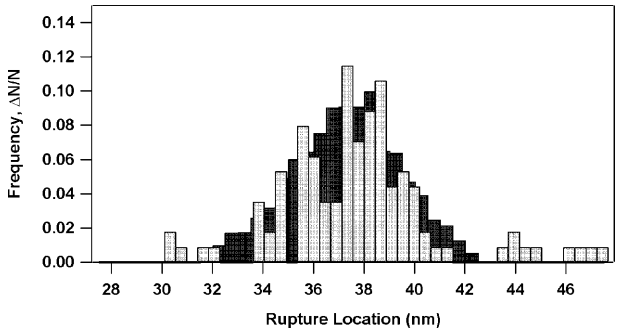

FIGURE 7 Experimental (*shaded bars*) and simulated (*solid bars*) length distributions for the specific interactions between tethered ConA and tethered mannose. For the simulation, the system included a single fixed-length tether on the AFM tip and a range of tether lengths (taken from the mass spectrometry data) on the substrate.

(Farago et al., 2002). Knots could have various effects, but principally they would move specific binding events out of the peak we have identified as specific binding in the length distributions, and may account, at least in part, for events having the rupture force associated with specific bond rupture at shorter lengths. They would not tend to move nonspecific events into the specific peak. The formation of a temporarily looped section of polymer would be expected to decrease the effective length of a tether and thus generate a wider variability of measured lengths than predicted from the angular dependence alone. A final possibility is that the tether may interact either with the ConA molecule, possibly by wrapping around the protein or with the AFM tip itself. This could also shorten the effective length of the polymer tether, however, these scenarios are less likely due to the requirement that the hydration shell surrounding the polymer would need to be disrupted before binding.

CONCLUSIONS

Through a combination of atomic force spectroscopy, mass spectroscopy, and Monte Carlo simulations we have shown that tethering both the protein and the ligand enables the high sensitivity determination of the rupture force required to separate a single ConA protein from its mannose ligand. In all, we report narrower force distributions than previously measured from which nonspecific binding has been largely eliminated through spatial isolation. In addition, the remaining force and location distribution widths have been understood even further through the angle analysis (i.e., the intrinsic distribution is narrower yet, and we have identified the leading source of error). Finally, this double-tethered approach can be used to validate the presence of a single-tethered functional molecule on the AFM tip. We consider these measurements to be crucial for developing an understanding of the molecular configurations of tethered molecules, a key requirement in the design of bioactive surfaces and a necessity for developing an understanding of biologically tethered proteins. In future experiments, this approach will be used to examine multivalent protein-ligand interactions using cells plated onto substrates that have been functionalized with tethered ligands. This will allow each functionalized tip to be characterized before being used to measure the forces associated with ligand binding to cell surface receptors imbedded in the membranes of living cells.

SUPPLEMENTARY MATERIAL

An online supplement to this article can be found by visiting BJ Online at http://www.biophysj.org.

We thank Stuart Lindsay and Christine Orme for useful discussions, Sharon Shields and Julio Camarero for mass spectrometry assistance, and Sal Zepeda and Scott McCall for assistance with data analysis.

This work was performed under the auspices of the U.S. Department of Energy by University of California, Lawrence Livermore National Laboratory under contract number W-7405-Eng-48.

REFERENCES

Benoit, M., D. Gabriel, G. Gerisch, and H. E. Gaub. 2000. Discrete interactions in cell adhesion measured by single-molecule force spectroscopy. *Nat. Cell Biol.* 2:313–317.

Butt, H. J., and M. Jaschke. 1995. Calculation of thermal noise in atomic force microscopy. *Nanotechnology.* 6:1–7.

Chang, K. C., and D. A. Hammer. 1999. The forward rate of binding of surface-tethered reactants: effect of relative motion between two surfaces. *Biophys. J.* 76:1280–1292.

Chen, A. L., and V. T. Moy. 2002. Single-molecule force measurements. (Review) B. P. Jena and J. K. H. Horber, editors. *Atomic Force Microscopy in Cell Biology.* 68:301–309.

Clausen-Schaumann, H., M. Seitz, R. Krautbauer, and H. E. Gaub. 2000. Force spectroscopy with single bio-molecules. (Review) *Curr. Opin. Chem. Biol.* 4:524–530.

Conti, M., G. Donati, G. Cianciolo, S. Stefoni, and B. Samori. 2002. Force spectroscopy study of the adhesion of plasma proteins to the surface of a dialysis membrane: role of the nanoscale surface hydrophobicity and topography. *J. Biomed. Mater. Res.* 61:370–379.

Davis, S. J., S. Ikemizu, E. J. Evans, L. Fugger, T. R. Bakker, and P. A. van der Merwe. 2003. The nature of molecular recognition by T cells. (Review) *Nat. Immunol.* 4:217–224.

Evans, E. 2001. Probing the relation between force - lifetime - and chemistry in single molecular bonds. (Review) *Annu. Rev. Biophys. Biomol. Struct.* 30:105–128.

Farago, O., Y. Kantor, and M. Kardar. 2002. Pulling knotted polymers. *Europhys. Lett.* 60:53–59.

Florin, E. L., V. T. Moy, and H. E. Gaub. 1994. Adhesion forces between individual ligand-receptor pairs. *Science.* 264:415–417.

Florin, E. L., M. Rief, H. Lehmann, M. Ludwig, C. Dornmair, V. T. Moy, and H. E. Gaub. 1995. Sensing specific molecular interactions with the atomic force microscope. *Biosens. Bioelectron.* 10:895–901.

Friedsam, C., A. K. Wehle, F. Kuhner, and H. E. Gaub. 2003. Dynamic single-molecule force spectroscopy: bond rupture analysis with variable spacer length. *Journal of Physics-Condensed Matter.* 15:S1709–S1723.

Gad, M., A. Itoh, and A. Ikai. 1997. Mapping cell wall polysaccharides of living microbial cells using atomic force microscopy. *Cell Biol. Int.* 21:697–706.

Grandbois, M., M. Beyer, M. Rief, H. Clausen-Schaumann, and H. E. Gaub. 1999. How strong is a covalent bond? *Science.* 283:1727–1730.

Hugel, T., and M. Seitz. 2001. The study of molecular interactions by AFM force spectroscopy. (Review) *Macromolecular Rapid Communications.* 22:989–1016.

Hutter, J. L., and J. Bechhoefer. 1993. Calibration of atomic-force microscope tips. *Rev. Sci. Instrum.* 64:3342.

Jeppesen, C., J. Y. Wong, T. L. Kuhl, J. N. Israelachvili, N. Mullah, S. Zalipsky, and C. M. Marques. 2001. Impact of polymer tether length on multiple ligand-receptor bond formation. *Science.* 293:465–468.

Kanellopoulos, P. N., P. A. Tucker, K. Pavlou, B. Agianian, and S. J. Hamodrakas. 1996. A triclinic crystal form of the lectin concanavalin a. *J. Struct. Biol.* 117:16–23.

Kienberger, F., C. Stroh, G. Kada, R. Moser, W. Baumgartner, V. Pastushenko, C. Rankl, U. Schmidt, H. Muller, E. Orlova, C. LeGrimellec, D. Drenckhahn, D. Blaas, and P. Hinterdorfer. 2003. Dynamic force microscopy imaging of native membranes. *Ultramicroscopy.* 97:229–237.

Lavigne, J. J., and E. V. Anslyn. 2001. Sensing a paradigm shift in the field of molecular recognition: from selective to differential receptors. (Review) *Angewandte Chemie-International Edition.* 40:3119–3130.

Liu, Y. Z., S. H. Leuba, and S. M. Lindsay. 1999. Relationship between stiffness and force in single molecule pulling experiments. *Langmuir*. 15:8547–8548.

Ludwig, M., V. T. Moy, M. Rief, E. L. Florin, and H. E. Gaub. 1994. Characterization of the adhesion force between avidin-functionalized AFM tips and biotinylated agarose beads. *Microscopy Microanalysis Microstructures*. 5:321–328.

Mann, D. A., M. Kanai, D. J. Maly, and L. L. Kiessling. 1998. Probing low affinity and multivalent interactions with surface plasmon resonance: ligands for concanavalin a. *J. Am. Chem. Soc*. 120:10575–10582.

McDonnell, J. M. 2001. Surface plasmon resonance: towards an understanding of the mechanisms of biological molecular recognition. (Review) *Curr. Opin. Chem. Biol*. 5:572–577.

Merkel, R. 2001. Force spectroscopy on single passive biomolecules and single biomolecular bonds. (Review) *Physics Reports-Review Section of Physics Letters*. 346:344–385.

Riener, C. K., C. M. Stroh, A. Ebner, C. Klampfl, A. A. Gall, C. Romanin, Y. L. Lyubchenko, P. Hinterdorfer, and H. J. Gruber. 2003. Simple test system for single molecule recognition force microscopy. *Anal. Chim. Acta*. 479:59–75.

Riper, J. W., R. A. Swerlick, and C. Zhu. 1998. Determining force dependence of two-dimensional receptor-ligand binding affinity by centrifugation. *Biophys. J*. 74:492–513.

Touhami, A., B. Hoffmann, A. Vasella, F. A. Denis, and Y. F. Dufrene. 2003. Probing specific lectin-carbohydrate interactions using atomic force microscopy imaging and force measurements. *Langmuir*. 19:1745–1751.

Varki, A. 1993. Biological roles of oligosaccharides: all of the theories are correct. *Glycobiology*. 3:97–130.

Wong, J. Y., T. L. Kuhl, J. N. Israelachvili, N. Mullah, and S. Zalipsky. 1997. Direct measurement of a tethered ligand-receptor interaction potential. *Science*. 275:820–822.

Zhao, Y. H., S. Chien, and S. Weinbaum. 2001. Dynamic contact forces on leukocyte microvilli and their penetration of the endothelial glycocalyx. *Biophys. J*. 80:1124–1140.

Zhu, C. 2000. Kinetics and mechanics of cell adhesion. (Review) *J. Biomech*. 33:23–33.

Zlatanova, J., S. M. Lindsay, and S. H. Leuba. 2000. Single molecule force spectroscopy in biology using the atomic force microscope. (Review) *Prog. Biophys. Mol. Biol*. 74:37–61.